ACS Photonics

Article

pubs.acs.org/journal/apchd5

Passive Parity-Time Symmetry in Organic Thin Film Waveguides

Yufei Jia,[†] Yixin Yan,[†] Sameer Vajjala Kesava,[‡] Enrique D. Gomez,[‡,§] and Noel C. Giebink*[,†]

[†]Department of Electrical Engineering, [‡]Department of Chemical Engineering, and [§]Materials Research Institute, The Pennsylvania State University, University Park, Pennsylvania 16802, United States

Supporting Information

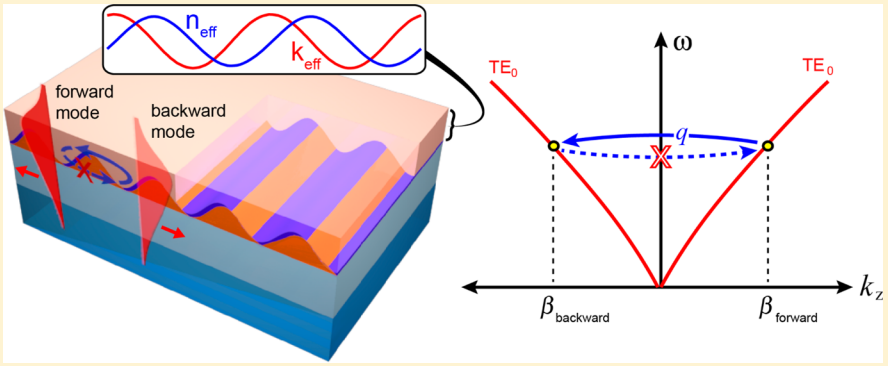

ABSTRACT: Periodic media are fundamentally important for controlling the flow of light in photonics. Recently, the emerging field of non-Hermitian optics has generalized the notion of periodic media to include a new class of materials that obey parity-time ($\mathcal{PT}$) symmetry, with real and imaginary refractive index variations that transform into one another upon spatial inversion, leading to a variety of unusual optical phenomena. Here, we introduce a simple approach based on interference lithography and oblique angle deposition to achieve $\mathcal{PT}$-symmetric modulation in the effective index of large area organic thin film waveguides with the functional form $\Delta\tilde{n}_{\mathrm{eff}}(z) \sim e^{iqz}$. Passive $\mathcal{PT}$ symmetry breaking is observed through asymmetry in the forward and backward diffraction of waveguided light that maximizes at the exceptional point, resulting in unidirectional reflectionless behavior that is visualized directly via leakage radiation microscopy. These results establish the basis for organic $\mathcal{PT}$ waveguide media that can be tuned for operation throughout the visible to near-infrared spectrum and provide a direct pathway to incorporate gain sufficient to achieve active $\mathcal{PT}$ symmetric lattices and gratings.

KEYWORDS: *parity-time symmetry, waveguide, thin film, organic photonics*

Synthetic photonic materials with independent spatial variation in their real and imaginary complex refractive index components have elicited widespread interest as a platform for exploring the physics and applications of parity-time ($\mathcal{PT}$) symmetry in optics.[1−9] Following the original observation by Bender and co-workers that non-Hermitian Hamiltonians can exhibit real energy spectra provided they remain unchanged under the combined operation of parity inversion ($\mathcal{P}$) and time reversal ($\mathcal{T}$),[10] much effort has focused on the optically analogous situation that arises when the refractive index spatial profile and its complex conjugate satisfy $\tilde{n}(\boldsymbol{r}) = \tilde{n}^*(-\boldsymbol{r})$.[1−4] This condition has been most widely explored using two-component coupled waveguides and microcavities with balanced gain and loss;[1,2,5,9,11,12] however, a continuing goal is to realize it in extended periodic systems (e.g., complex gratings and lattices),[4,6,8,13,14] where unusual optical phenomena such as unidirectional invisibility have been theoretically predicted together with a host of new device applications.[3,6−8,15−18]

Recent progress toward this goal has demonstrated complex refractive index ($\tilde{n} = n + ik$) variation that approximates the passive $\mathcal{PT}$ symmetric profile $\Delta\tilde{n}(z) \sim [\Delta n \cos(qz) + i\Delta k \sin(qz)]$ in a multilayer organic thin film[19] as well as in the effective index of a silicon-on-insulator waveguide.[6] The latter result is notable because it is achieved on a microscale platform relevant for photonic integration; however, by the same measure, it is difficult to scale to larger areas and to incorporate active gain that would enable a wider range of $\mathcal{PT}$ predictions to be explored.

Here, we introduce a simple route to construct passive $\mathcal{PT}$ symmetry in the modal effective index of large area ($\sim$cm^2) organic thin film waveguides fabricated from photoresist and the blue pigment copper phthalocyanine (CuPc) through a combination of interference lithography and oblique angle deposition. Kretschmann coupling to the fundamental transverse electric (TE) mode in Littrow yields strong asymmetry in the diffracted first order for left versus right incidence that maximizes when $\Delta n = \Delta k$, marking an exceptional point transition to the broken $\mathcal{PT}$ phase that is supported by modeling. These results establish organic small molecules and polymers as a versatile platform to create $\mathcal{PT}$ periodic optical

Received: December 8, 2014
Published: January 15, 2015

DOI: 10.1021/ph500459j
ACS Photonics 2015, 2, 319−325

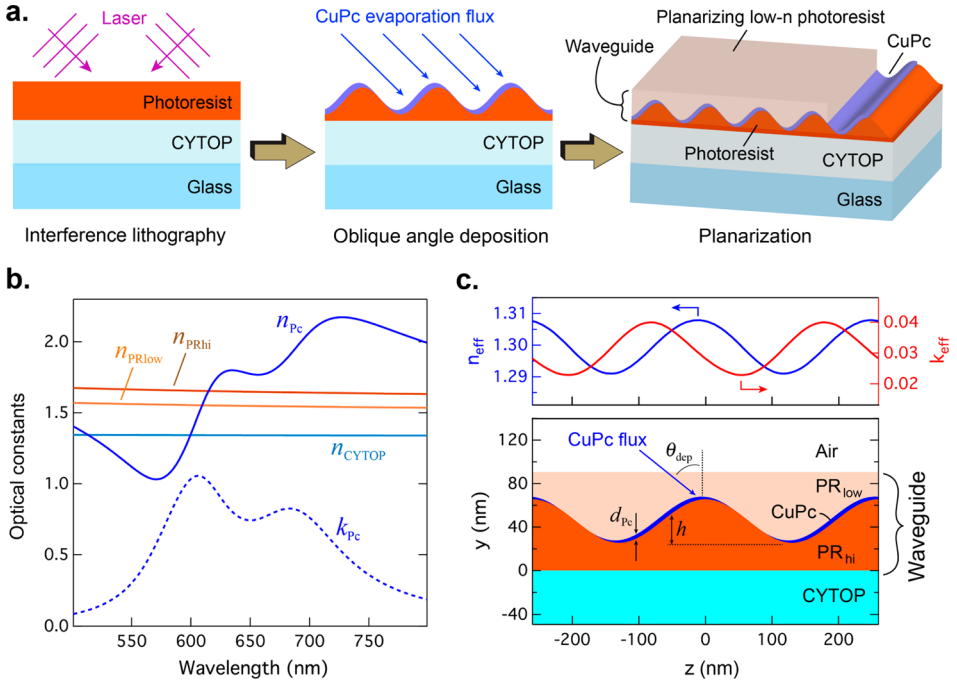

Figure 1. (a) Schematic of the waveguide fabrication method. Interference lithography is used to pattern a sinusoidal surface relief profile into a thin layer of photoresist followed by oblique angle evaporation of copper phthalocyanine (CuPc) to selectively coat one side of the grating facets. The structure is completed by spin-coating on a second layer of photoresist (PR_{low}), diluted with poly(methyl methacrylate) to lower its refractive index. The low index fluoropolymer interlayer (CYTOP) serves to enable evanescent in- and out-coupling to the waveguide mode from the glass substrate. (b) Optical constant dispersions of the materials used to construct the waveguide; subscripts Pc and PR denote copper phthalocyanine and photoresist, respectively. (c) Waveguide composition calculated to support the fundamental leaky transverse electric mode together with its corresponding position-dependent complex effective index $\tilde{n}_{eff} = n_{eff} + ik_{eff}$ displayed in the top panel.

materials and provide a direct path to incorporate gain sufficient to realize active $\mathcal{PT}$ symmetric lattices in one and two dimensions.

WAVEGUIDE ARCHITECTURE

Figure 1a presents a process flow diagram illustrating the waveguide architecture and fabrication approach based on the materials and optical constant dispersions shown in Figure 1b. Interference lithography is used to write a sinusoidal grating profile with period Λ into a thin film of photoresist followed by oblique angle deposition of high extinction coefficient CuPc to lightly coat the "windward" grating facets. The waveguide is then completed by planarizing it with a top layer of photoresist that is formulated to have a slightly lower refractive index than that of the sinusoidally patterned underlying photoresist. Because this underlayer is hard baked and CuPc is insoluble in the liquid photoresist, the integrity of the internal sinusoidal structure is maintained during planarization.

This arrangement results in a modal effective index with a sinusoidally varying real part that follows the relative thickness variation between high and low index photoresist, and an imaginary part (loss) that varies in proportion to the local CuPc thickness (see Figure 1c). Because the CuPc thickness maximizes on the "windward" grating faces but is negligible on the "leeward" faces, the loss modulation is shifted by roughly a quarter period from the real index modulation, thereby approximating an effective index profile of the form $\Delta\tilde{n}_{eff}(z) \approx (\Delta n_{eff}/2)[1 + \cos(qz)] + i(\Delta k_{eff}/2)[1 - \sin(qz)]$ for the fundamental guided mode. Access to this mode is accomplished by separating the composite waveguide from the glass substrate with a d_{low} = 350 nm thick film of low refractive index fluoropolymer (CYTOP). The thickness of this interlayer determines the amount of evanescent modal overlap with the glass substrate and thus enables efficient (resonant) in- and out-coupling from the waveguide to radiation modes in the glass substrate that have the same in-plane wavevector.

The essential aspects of this effective index modulation scheme can be understood using a simple analytical model outlined in Figure 1c based on a sinusoidal surface relief profile, $h(z) = (h_0/2)[1 + \cos(qz)]$, defined in the bottom photoresist by interference lithography (here h_0 is the peak to valley height and $q = 2\pi/\Lambda$ is the grating vector). Assuming a unity sticking coefficient for CuPc molecules incident in a collimated flux onto the grating at angle θ_{dep}, the vertical thickness of deposited CuPc is $d_{PC}(z) = d^0_{PC}[\cos\theta_{dep} - \sin\theta_{dep}\sin(qz)\, h_0 q/2]$, where d^0_{PC} is the nominal thickness that would result from the same flux on a flat surface at normal incidence. Details of the derivation are provided in the Supporting Information. In this line-of-sight deposition model, the onset of shadowing (and thus abrupt discontinuities in the CuPc layer) occurs when $\tan\theta_{dep} = 2/h_0 q$, which corresponds to a deposition flux oriented parallel to the maximum slope of the grating facets. Depositing at this threshold angle simplifies the expression for CuPc thickness to $d_{PC}(z) = d^0_{PC}\cos\theta_{dep}[1 - \sin(qz)]$ and, thus, yields a sinusoidal CuPc profile that fully extinguishes on the leeward grating facets and is phase-shifted from the photoresist grating by exactly one-quarter period.

Figure 1c shows the predicted composition for a 90 nm thick waveguide designed to support the (leaky) fundamental transverse electric mode at a free space wavelength λ = 640 nm. Taking Λ = 260 nm, h_0 = 40 nm, d^0_{PC} = 5 nm, and θ_{dep} = 65° together with the refractive indices provided in Figure 1b, the complex modal effective index is computed at each position

DOI: 10.1021/ph500459j
ACS Photonics 2015, 2, 319−325

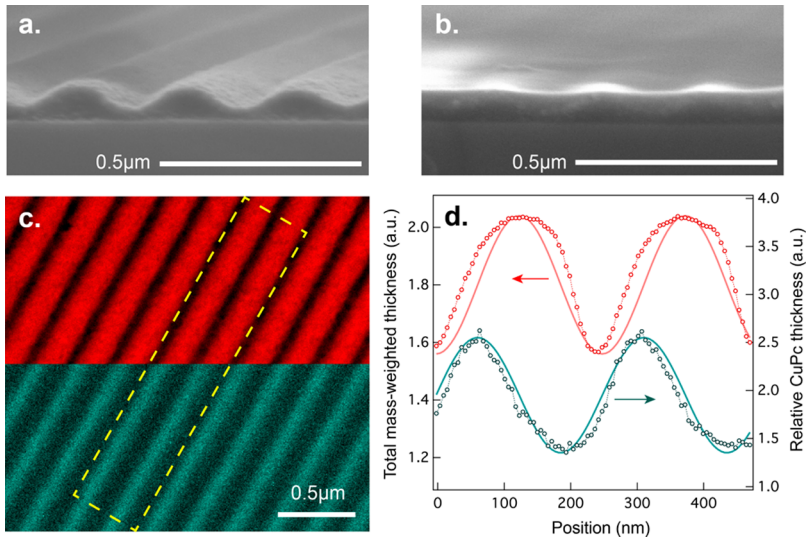

Figure 2. Cross-sectional scanning electron microscope images of a typical CuPc-coated photoresist grating before (a) and after (b) planarization with the top photoresist layer. Faint contrast between the upper and lower photoresist layers remains visible in (b), confirming that the internal grating structure is maintained. (c) Bright field (zero-loss) image and Cu elemental map generated from energy-filtered TEM micrographs of a grating similar to that shown in (a), with d^0_{PC} = 15 nm of CuPc deposited at θ_{dep} = 65°. The top half of the image is a bright field micrograph, where intensities are proportional to the total mass-weighted thickness. The bottom half (of the same image) shows a Cu elemental map generated from energy-filtered TEM near the Cu L_3 edge (931 eV), where intensities are proportional to the thickness of CuPc. (d) Integrated line scans of the bright field image (dark red circles) and Cu elemental map (dark green circles) acquired within the dashed yellow rectangle along the grating vector in (c). Analytical cosine and sine functions (solid lines) are overlaid on the data for reference to the targeted thickness functional forms.

along the waveguide using a transfer matrix model[20] and plotted in the upper panel of Figure 1c. There, the real and imaginary effective index components exhibit near-sinusoidal variation as expected from the waveguide composition, phase-shifted by $\pi/2$ from one another with approximately equal peak to valley modulation depth $\Delta n_{eff} \approx \Delta k_{eff} \approx 0.017$. The constant offset of k_{eff} independent of CuPc thickness reflects the leaky nature of this mode due to outcoupling into the glass substrate. Weak modal confinement is similarly evident from the low average effective index $\langle n_{eff} \rangle \approx 1.3$ and is advantageous from a design standpoint because it minimizes variation of the modal intensity profile over the waveguide cross-section and thereby evenly weights the index contribution of each component material.

Figure 2a,b shows scanning electron micrographs of a typical composite waveguide (fabricated on Si for imaging purposes) before and after planarization. The sinusoidal profile of the underlying photoresist is clearly evident in Figure 2a and remains discernible in Figure 2b beneath the planarizing top layer. To assess the CuPc deposition profile, one of the coated gratings was floated off of its substrate and imaged using energy-filtered transmission electron microscopy (EFTEM). The top half of Figure 2c displays a bright field image (zero-loss micrograph) of the coated gratings, where contrast is dominated by the thickness of the photoresist. The bottom half of Figure 2c shows a Cu elemental map obtained through the standard three window method from EFTEM images near the Cu L3 edge (931 eV).[21,22] Intensities in the Cu elemental map are proportional to the amount of Cu. It is readily apparent from this image that the CuPc thickness (proportional to the EFTEM intensity) varies in approximately sinusoidal fashion and that the CuPc thickness maxima are offset from the photoresist grating by approximately one-quarter period. This qualitative assessment is confirmed by line scans of each image shown in Figure 2d, where the relative CuPc thickness (dark green) is well-approximated by a sine function with period Λ = 260 nm and the bright field line scan (dark red) is slightly skewed from a cosine function because it is proportional to the total mass density in the electron path (i.e., including both photoresist and CuPc).

■ PASSIVE $\mathcal{PT}$ SYMMETRY BREAKING

The complex index profile of the waveguides was subsequently explored via Kretschmann-coupled diffraction in Littrow as illustrated schematically in Figure 3a. As shown in the inset, when the in-plane component of the incident wavevector in the glass substrate ($k_{zi} = 2\pi n_{gls} \sin \theta_{inc}/\lambda$) matches the modal propagation constant ($\beta = 2\pi n_{eff}/\lambda$), light is resonantly in-coupled into the waveguide. If the grating momentum q is set to the Bragg condition (i.e., $q = 2\beta$), then the forward and backward modes are coupled, giving rise to a −1 order Littrow diffracted beam.

In the limit of weak evanescent coupling to the waveguide (e.g., a thick CYTOP layer), the Littrow diffraction process can be pictured as the sequence of evanescent in-coupling followed by grating reflection into the reverse-going waveguide mode and subsequent evanescent out-coupling (see Figure 3a). Measuring the −1 order diffraction efficiency for left and right incident light thus provides a proxy probe of the forward- and backward-going modal reflectivity within the waveguide. For a waveguide with $\mathcal{PT}$-symmetric effective index modulation of the form $\Delta n_{eff}(z) \propto \cos(qz) + i \sin(qz) = e^{iqz}$, the scattering potential is one-sided and the reflectivity in the reverse direction vanishes, as outlined in Figure 3b, leading to an expected asymmetry in the forward/backward diffraction efficiencies (D_F and D_B, respectively).[6]

Figure 4a presents the result of this measurement using a TE-polarized, λ = 640 nm probe beam as a function of incidence angle in the glass substrate for a 90 ± 5 nm thick waveguide (Λ = 260 nm) in which CuPc has been omitted to yield a purely real effective index modulation. Here, D_F and D_B peak with

DOI: 10.1021/ph500459j
ACS Photonics 2015, 2, 319−325

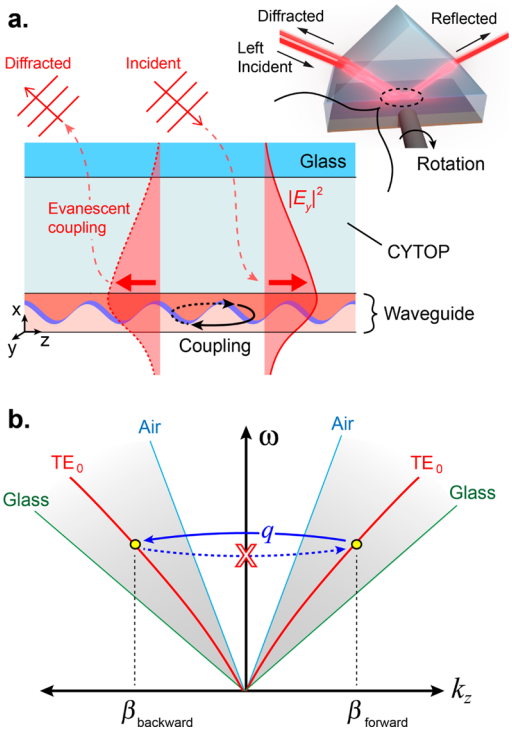

Figure 3. (a) Diagram showing the optical measurement setup, where a laser beam is Kretschmann-coupled into the leaky TE_0 mode supported by the composite waveguide layer. The intensity of the 0 order reflected and −1 order diffracted beam is measured as a function of incidence angle for forward and backward illumination corresponding to light incident on the left and right sides of the prism, respectively. (b) Dispersion diagram illustrating the process of unidirectional scattering within the complex index modulated waveguide that occurs at its exceptional point. Light in-coupled into the forward-going mode can scatter into the backward going mode, giving rise to a Littrow-diffracted beam but not vice versa, owing to the one-sided Fourier transform of the grating potential.

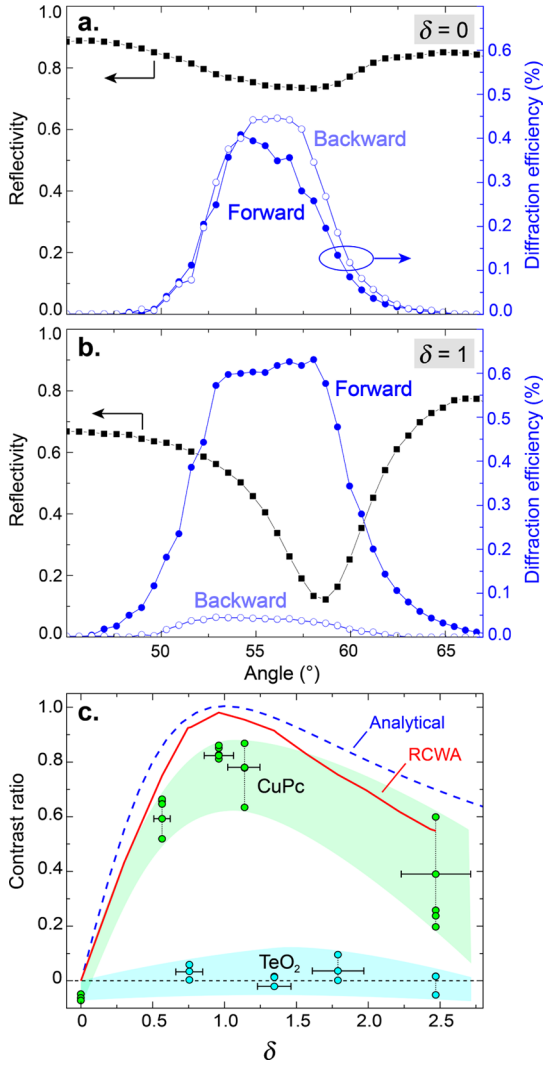

Figure 4. (a) Reflectivity and −1 order diffraction efficiencies measured as a function of incidence angle (in the glass substrate) for a bare waveguide with no CuPc. The diffracted intensities for forward and backward incidence peak near the Littrow condition ($\theta_{inc} \sim 56°$), which is designed to coincide with resonant in-coupling to the waveguide mode marked by the reflectivity dip (the reflectivity is identical for both incidence directions). (b) The same measurement carried out for a waveguide with CuPc (d^0_{PC} = 6 nm, θ_{dep} = 55°) targeted to achieve $\delta \approx 1$. As compared to (a), the reflectivity dip in this case is larger owing to absorption by the CuPc, whereas a strong asymmetry in forward/backward Littrow diffraction efficiencies is observed. The angular offset between the reflectivity minimum and the diffraction efficiency peak in both (a) and (b) is due to a slight mismatch between the grating momentum and modal propagation constant of the waveguides (i.e., q is smaller than 2β). (c) Forward/backward diffraction efficiency contrast ratio averaged over the Littrow peak (±1°) for a large number of waveguides with varying CuPc thickness (filled green circles) and plotted vs the effective index asymmetry parameter, $\delta = \Delta k_{eff}/\Delta n_{eff}$, estimated from transfer matrix modeling of each structure. Error bars in δ reflect uncertainty in the oblique deposition angle and nominal CuPc thickness. The data exhibit a peak in diffraction contrast at $\delta = 1$ that is qualitatively consistent with approximate analytical coupled mode theory (blue dashed line) and rigorous RCWA diffraction modeling (red line) of the structures that were actually fabricated. Control waveguides in which CuPc is replaced with similar thicknesses of nonabsorbing TeO_2 (filled cyan circles) display no statistically significant contrast. Light green and cyan shaded regions indicate the range of results obtained for multiple different samples measured on different days.

similar magnitudes, exhibiting bidirectional symmetry, as expected near the resonant in-coupling angle $\theta_{inc} \sim 56°$ that corresponds to the reflectivity minimum (black curve). In stark contrast, adding CuPc (d^0_{PC} = 6 nm, θ_{dep} = 55°) into the same structure to achieve the condition $\Delta n_{eff} \approx \Delta k_{eff}$ leads to a strong asymmetry in Figure 4b, where D_F is enhanced and D_B is almost entirely suppressed.

As shown previously,[3,6,15] this behavior can be understood on the basis of coupled mode theory in terms of the forward and backward propagating modal amplitudes [$A(z)$ and $B(z)$, respectively] and the normalized index asymmetry parameter, $\delta = \Delta k_{eff}/\Delta n_{eff}$. Assuming weak evanescent coupling as above to preserve the notion of well-defined waveguide modes, the incident plane wave amplitude E_{inc} on resonance is related to the forward-going amplitude A by the same complex coefficient, C, that relates the backward-going amplitude B to the outgoing diffracted wave E_{dif}, owing to time-reversal symmetry. Consequently, the forward Littrow diffraction efficiency $D_F = |E_{dif}/E_{inc}|^2 = |CB/CA|^2$ is approximately equal to the forward-going modal reflectivity in the waveguide $R_F = |B/A|^2$ since there is no solid angle change between R and D in Littrow. Similarly, $D_B \approx R_B$, and thus, the backward to forward Littrow diffraction efficiency ratio, $D_B/D_F \approx [(1 - \delta)/(1 + \delta)]^2$, is the same as that for R_B/R_F derived previously.[6]

DOI: 10.1021/ph500459j
ACS Photonics 2015, 2, 319−325

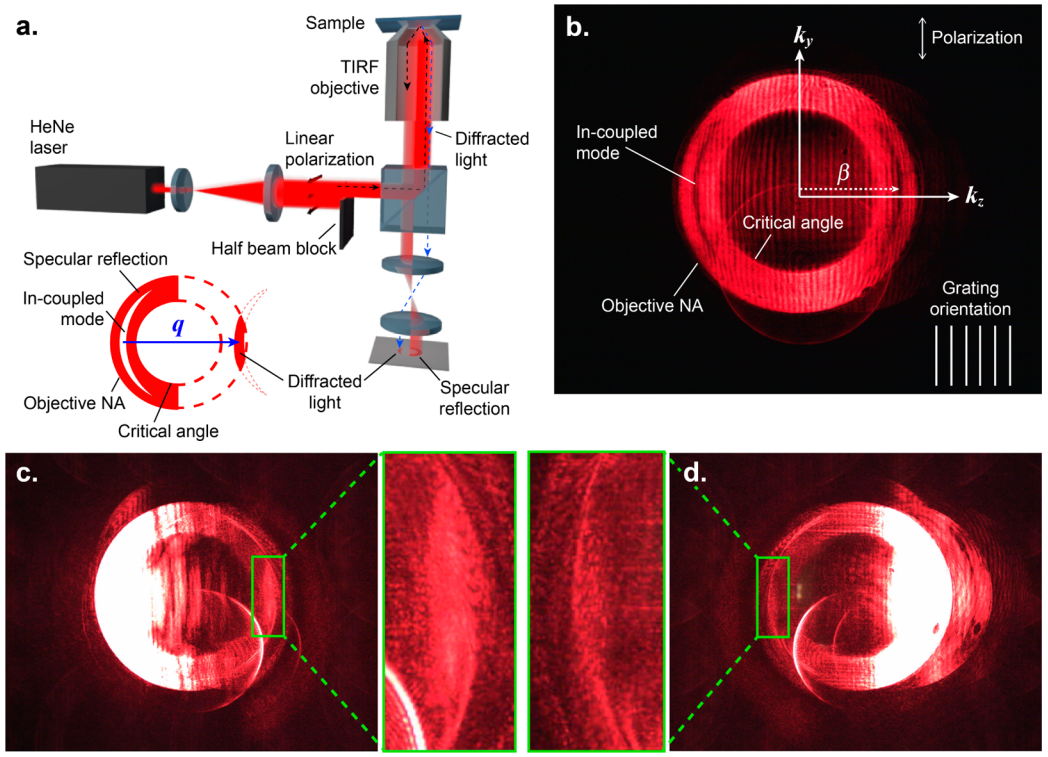

Figure 5. (a) Experimental configuration used to image mode coupling and diffraction from the waveguides using a total internal reflection objective and a 4f optical system set to image its back focal plane. Dashed lines follow the real-space light path whereas the inset illustrates the scattering process in *k*-space. (b) Image of a typical sample under full beam illumination (no beam block), with light coupled into forward and backward-going modes that correspond to the dark slits on the left and right, respectively. Coupling does not occur at the top and bottom of the ring since this corresponds to transverse magnetic illumination; the faint ring displaced toward the lower half of the image arises from the ghost reflection of a wedged beam splitter. (c, d) Images of a $\delta \approx 1$ CuPc waveguide under half beam illumination, demonstrating diffraction for left-going light in (c) but not for right-going light in (d). The exposure of these images is increased by a factor of 10 relative to that in (b) due to the low diffraction efficiency (<1%) of the waveguide. Analogous images obtained for a control waveguide with no CuPc display symmetric diffraction and are provided in the Supporting Information.

This relationship is summarized together with the experimental data in Figure 4c by plotting the diffraction efficiency contrast ratio, $CR = |D_F - D_B|/(D_F + D_B)$. The circular data points indicate the contrast ratios measured for different sets of waveguides with varying CuPc thickness in the range $0 < d_{PC}^0 < 15$ nm to tune δ. In spite of the scatter arising from sample-to-sample variation, these data exhibit a clear maximum in the vicinity of $\delta = 1$ that marks an exceptional point transition from the exact to the broken $\mathcal{PT}$ phase, analogous to that in balanced gain and loss active $\mathcal{PT}$ systems except with rescaled, subunity modulus scattering matrix eigenvalues due to the net loss of this passive system.[2,6] The observed trend is in qualitative agreement with that predicted by coupled mode theory outlined above [$CR = 2\delta/(1 + \delta^2)$; blue dashed line][6,19] as well as with rigorous coupled wave (RCWA) numerical diffraction modeling (solid red line).[23,24] By contrast, replacing the absorbing CuPc with equivalently deposited, nonabsorbing TeO_2 ($n = 2.18$ at $\lambda = 640$ nm) in a series of control samples to introduce spatial asymmetry in Δn_{eff} while maintaining $\Delta k_{eff} \approx 0$ yields negligible asymmetry between D_F and D_B (filled cyan data points; see the Supporting Information for details).

IMAGING UNIDIRECTIONAL DIFFRACTION

The diffraction asymmetry is demonstrated visually in Figure 5, where an inverted microscope equipped with a total internal reflection objective (TIRF, NA = 1.49) is used to directly image the modal in-coupling and resultant diffraction of a $\delta = 1$ CuPc sample fabricated on a glass coverslip. As shown schematically in Figure 5a, a linearly polarized TEM_{00} laser beam ($\lambda = 633$ nm) is expanded to fill the rear aperture of the index-matched objective, recollected through a beam splitter, and imaged in the microscope Fourier plane to map the intensity distribution in k-space.[25] Figure 5b displays a typical image, which consists of a ring of light confined between wavevectors corresponding to the glass/air critical angle and the objective numerical aperture. Dark slits on either side of the ring result from light that is coupled into the forward/backward-going waveguide modes and lost due to absorption and random scattering.

Unidirectional diffraction from the waveguide is anticipated according to the inset *k*-space diagram in Figure 5a and is clearly evident in Figure 5c,d. In these images, an opaque card is inserted to block half of the expanded laser beam (see Figure 5a) to eliminate specularly reflected light from one direction, thereby enabling the weaker diffracted light (which essentially constitutes a retro-reflection when $q = 2\beta$) to be observed. Blocking the left or right half of the beam in Figure 5c,d thus selects whether light is coupled into forward or backward going waveguide modes, respectively. Consistent with the prism-based measurements in Figure 4b, the expected diffraction signature is observed for the forward-going case (Figure 5c) but is absent in the backward-going case (Figure 5d), thus, visually confirming the unidirectional reflectionless behavior that manifests at the $\mathcal{PT}$ symmetry breaking point. Although the focus here is on propagation parallel to the grating vector, we

DOI: 10.1021/ph500459j
ACS Photonics 2015, 2, 319−325

anticipate that this microscopy approach will prove particularly useful in subsequent investigations for observing the real space and k-space evolution of light propagating orthogonal to the grating vector in a one-dimensional $\mathcal{PT}$ lattice configuration (or straightforwardly a 2D lattice using the same fabrication approach), where power oscillations and unusual diffraction effects have been predicted.[8,13,14,26]

CONCLUSION

In conclusion, we have demonstrated a simple and robust approach to realize large area organic thin film waveguides that exhibit $\mathcal{PT}$-symmetric effective index modulation $\Delta\tilde{n}_{\mathrm{eff}}(z) \sim e^{iqz}$ for the fundamental mode. Passive $\mathcal{PT}$ symmetry breaking is confirmed from the evolution of asymmetric forward and backward Littrow diffraction efficiencies with varying complex index contrast and unidirectional modal reflectivity at the exceptional point has been visualized directly using TIRF microscopy. Looking forward, we expect that this architecture can be extended to achieve active $\mathcal{PT}$ symmetry by suitably incorporating an organic small molecule or polymer gain medium[27] to create similar effective index profiles with balanced gain and loss. This prospect, coupled with the synthetic (spectral) freedom of organic materials and established soft lithography techniques[28,29] to pattern and integrate them with inorganic photonic structures make the complex index modulation platform developed here a promising and technologically relevant route to explore and exploit $\mathcal{PT}$ phenomena in optics.

METHODS

Modeling. Modal propagation constants were calculated for planar waveguide architectures using transfer matrices and the argument principle method.[20] Local effective indices of the composite waveguide structure were estimated at each axial position, z, via the propagation constant calculated for a corresponding infinite planar waveguide with the same layer structure. Rigorous coupled wave analysis (RCWA) diffraction modeling[23,24] was carried out maintaining 20 field harmonics with the composite waveguide layer divided into 320 slices.

Sample Fabrication. Composite waveguides were fabricated beginning with an approximately 100 nm thick layer of S1800 photoresist that was subsequently exposed using an interference lithography system (λ = 405 nm) in a Lloyd mirror configuration.[30] The resultant gratings were hard-baked (5 min, 150 °C) and loaded into a thermal evaporator, oriented appropriately for oblique angle deposition of CuPc with nominal film thickness (d^0_{PC}) monitored via a quartz crystal microbalance. The waveguides were completed by spin-coating on a planarization layer consisting of S1800 photoresist mixed with 4 wt % poly(methyl methacrylate) dissolved in toluene, resulting in a film refractive index n = 1.55 at λ = 640 nm. Control experiments verified that CuPc is insoluble in this final photoresist mixture and does not wash off during the planarization process. Waveguide samples used for SEM imaging were fabricated on Si substrates, whereas those used for optical measurements were fabricated on B270 glass with an approximately 350 nm thick CYTOP fluoropolymer interlayer (Asahi Glass) to enable evanescent coupling to the waveguide mode.

Measurements and Data Analysis. Refractive index dispersions of each component material were determined using variable angle spectroscopic ellipsometry. Samples for TEM experiments were prepared by floating off CuPc-coated photoresist gratings in distilled water. Films were then picked up on bare copper TEM grids. The samples were vacuum-dried for 24 h at room temperature. TEM experiments were conducted on a JEOL LaB_6 at the Materials Characterization Lab of the Pennsylvania State University. The standard three-window method was used to obtain copper maps from energy-filtered micrographs near the Cu L3 edge (931 eV).[22] Reflectivity and diffraction measurements were carried out using a pair of automated rotation stages with a TE-polarized, λ = 640 nm laser incident on the sample in the Kretschmann configuration via a prism that was coupled to the back of the substrate with index matching fluid (Cargille Laboratories). The beam was chopped and detected synchronously in reflection/diffraction using a Si photodiode and a lock-in amplifier. Prism reflections are corrected for in the data analysis to determine the internal reflectivity/diffraction efficiencies within the glass substrate according to, for example, $R_{\mathrm{int}} = R_{\mathrm{meas}}/(T_{\mathrm{AG}}T_{\mathrm{GA}})$, where T_{AG} and T_{GA} are the appropriate (angle-dependent) air to glass and glass to air prism Fresnel transmittances, respectively. Leakage radiation microscopy was carried out using an Olympus IX-73 inverted microscope equipped with an NA = 1.49, 100× magnification TIRF immersion objective and a CCD camera.

ASSOCIATED CONTENT

Supporting Information

The supporting material details the derivation of the oblique angle deposition model and provides angular diffraction data collected for the series of control waveguides in which TeO_2 is substituted for CuPc. Leakage radiation microscopy images showing symmetric diffraction for control waveguides with no CuPc are also included. This material is available free of charge via the Internet at http://pubs.acs.org.

AUTHOR INFORMATION

Corresponding Author

*E-mail: ncg2@psu.edu.

Notes

The authors declare no competing financial interest.

ACKNOWLEDGMENTS

This work was supported by the Air Force Office of Scientific Research Young Investigator Program. SVK and EDG acknowledge financial support from NSF under Award DMR-1056199.

REFERENCES

(1) Rueter, C. E.; Makris, K. G.; El-Ganainy, R.; Christodoulides, D. N.; Segev, M.; Kip, D. Observation of parity-time symmetry in optics. *Nat. Phys.* **2010**, *6*, 192−195.

(2) Guo, A.; Salamo, G. J.; Duchesne, D.; Morandotti, R.; Volatier-Ravat, M.; Aimez, V.; Siviloglou, G. A.; Christodoulides, D. N. Observation of PT-Symmetry Breaking in Complex Optical Potentials. *Phys. Rev. Lett.* **2009**, *103*, 093902.

(3) Lin, Z.; Ramezani, H.; Eichelkraut, T.; Kottos, T.; Cao, H.; Christodoulides, D. N. Unidirectional Invisibility Induced by PT-Symmetric Periodic Structures. *Phys. Rev. Lett.* **2011**, *106*, 213901.

(4) Regensburger, A.; Bersch, C.; Miri, M.-A.; Onishchukov, G.; Christodoulides, D. N.; Peschel, U. Parity-time synthetic photonic lattices. *Nature* **2012**, *488*, 167−171.

(5) Hodaei, H.; Miri, M.-A.; Heinrich, M.; Christodoulides, D. N.; Khajavikhan, M. Parity-time−symmetric microring lasers. *Science* **2014**, *346*, 975−978.

DOI: 10.1021/ph500459j
ACS Photonics 2015, 2, 319−325

(6) Feng, L.; Xu, Y.-L.; Fegadolli, W. S.; Lu, M.-H.; Oliveira, J. E. B.; Almeida, V. R.; Chen, Y.-F.; Scherer, A. Experimental demonstration of a unidirectional reflectionless parity-time metamaterial at optical frequencies. *Nat. Mater.* **2013**, *12*, 108−113.
(7) Feng, L.; Wong, Z. J.; Ma, R.-M.; Wang, Y.; Zhang, X. Single-mode laser by parity-time symmetry breaking. *Science* **2014**, *346*, 972−975.
(8) Makris, K. G.; El-Ganainy, R.; Christodoulides, D. N.; Musslimani, Z. H. Beam dynamics in PT symmetric optical lattices. *Phys. Rev. Lett.* **2008**, *100*, 103904.
(9) Peng, B.; Ozdemir, S. K.; Lei, F.; Monifi, F.; Gianfreda, M.; Long, G. L.; Fan, S.; Nori, F.; Bender, C. M.; Yang, L. Parity-time-symmetric whispering-gallery microcavities. *Nat. Phys.* **2014**, *10*, 394−398.
(10) Bender, C. M.; Boettcher, S. Real spectra in non-Hermitian Hamiltonians having PT symmetry. *Phys. Rev. Lett.* **1998**, *80*, 5243−5246.
(11) Chang, L.; Jiang, X.; Hua, S.; Yang, C.; Wen, J.; Jiang, L.; Li, G.; Wang, G.; Xiao, M. Parity-time symmetry and variable optical isolation in active-passive-coupled microresonators. *Nat. Photonics* **2014**, *8*, 524−529.
(12) Peng, B.; Özdemir, Ş. K.; Rotter, S.; Yilmaz, H.; Liertzer, M.; Monifi, F.; Bender, C. M.; Nori, F.; Yang, L. Loss-induced suppression and revival of lasing. *Science* **2014**, *346*, 328−332.
(13) Makris, K. G.; El-Ganainy, R.; Christodoulides, D. N.; Musslimani, Z. H. PT-symmetric optical lattices. *Phys. Rev. A* **2010**, *81*, 063807.
(14) Makris, K. G.; El-Ganainy, R.; Christodoulides, D. N.; Musslimani, Z. H. PT-Symmetric Periodic Optical Potentials. *Int. J. Theor. Phys.* **2011**, *50*, 1019−1041.
(15) Kulishov, M.; Laniel, J. M.; Belanger, N.; Azana, J.; Plant, D. V. Nonreciprocal waveguide Bragg gratings. *Opt. Express* **2005**, *13*, 3068−3078.
(16) Kulishov, M.; Laniel, J. M.; Belanger, N.; Plant, D. V. Trapping light in a ring resonator using a grating-assisted coupler with asymmetric transmission. *Opt. Express* **2005**, *13*, 3567−3578.
(17) Kulishov, M.; Kress, B.; Slavik, R. Resonant cavities based on Parity-Time-symmetric diffractive gratings. *Opt. Express* **2013**, *21*, 9473−9483.
(18) Feng, L.; Ayache, M.; Huang, J.; Xu, Y.-L.; Lu, M.-H.; Chen, Y.-F.; Fainman, Y.; Scherer, A. Nonreciprocal Light Propagation in a Silicon Photonic Circuit. *Science* **2011**, *333*, 729−733.
(19) Yan, Y.; Giebink, N. C. Passive PT Symmetry in Organic Composite Films via Complex Refractive Index Modulation. *Adv. Opt. Mater.* **2014**, *2*, 423−427.
(20) Anemogiannis, E.; Glytsis, E. N. Multilayer waveguides - Efficient numerical analysis of general structures. *J. Lightwave Technol.* **1992**, *10*, 1344−1351.
(21) Kozub, D. R.; Vakhshouri, K.; Orme, L. M.; Wang, C.; Hexemer, A.; Gomez, E. D. Polymer Crystallization of Partially Miscible Polythiophene/Fullerene Mixtures Controls Morphology. *Macromolecules* **2011**, *44*, 5722−5726.
(22) Egerton, R. F. *Electron Energy-Loss Spectroscopy in the Electron Microscope*. 3rd ed.; Springer Verlag: 2011.
(23) Moharam, M. G.; Grann, E. B.; Pommet, D. A.; Gaylord, T. K. Formulation for stable and efficient implementation of the rigorous coupled-wave analysis of binary gratings. *J. Opt. Soc. Am. A* **1995**, *12*, 1068−1076.
(24) Moharam, M. G.; Pommet, D. A.; Grann, E. B.; Gaylord, T. K. Stable implementation of the rigorous coupled-wave analysis for surface-relief gratings: enhanced transmittance matrix approach. *J. Opt. Soc. Am. A* **1995**, *12*, 1077.
(25) Grandidier, J.; Des Francs, G. C.; Massenot, S.; Bouhelier, A.; Markey, L.; Weeber, J. C.; Dereux, A. Leakage radiation microscopy of surface plasmon coupled emission: investigation of gain-assisted propagation in an integrated plasmonic waveguide. *J. Microsc.* **2010**, *239*, 167−172.
(26) Longhi, S. Bloch Oscillations in Complex Crystals with PT Symmetry. *Phys. Rev. Lett.* **2009**, *103*, 123601.
(27) Samuel, I. D. W.; Turnbull, G. A. Organic semiconductor lasers. *Chem. Rev.* **2007**, *107*, 1272−1295.
(28) Carlson, A.; Bowen, A. M.; Huang, Y.; Nuzzo, R. G.; Rogers, J. A. Transfer Printing Techniques for Materials Assembly and Micro/Nanodevice Fabrication. *Adv. Mater.* **2012**, *24*, 5284−5318.
(29) Rogers, J. A.; Lee, H. H. *Unconventional nanopatterning techniques and applications*. Wiley: New York, 2009.
(30) Lu, C.; Lipson, R. H. Interference lithography: a powerful tool for fabricating periodic structures. *Laser & Photon. Rev.* **2010**, *4*, 568−580.

DOI: 10.1021/ph500459j
ACS Photonics 2015, 2, 319−325